Journal of Alloys and Compounds 506 (2010) 136–140

Contents lists available at ScienceDirect

Journal of Alloys and Compounds

journal homepage: www.elsevier.com/locate/jallcom

One-pot solvothermal syntheses and magnetic properties of graphene-based magnetic nanocomposites

Xiaoping Shen [a,*], Jili Wu [a], Song Bai [a], Hu Zhou [b]

[a] School of Chemistry and Chemical Engineering, Jiangsu University, Zhenjiang 212013, China
[b] School of Material Science and Engineering, Jiangsu University of Science and Technology, Zhenjiang 212003, China

ARTICLE INFO

Article history:
Received 20 May 2010
Received in revised form 20 June 2010
Accepted 24 June 2010
Available online 3 July 2010

Keywords:
Graphene
Magnetite
Synthesis
Nanocomposite
Magnetic properties

ABSTRACT

In this study, graphene-based magnetic nanocomposites (graphene/Fe_3O_4 and graphene oxide/Fe_3O_4) have been prepared via a facile and effective one-pot solvothermal method. X-ray diffraction (XRD), transmission electron microscopy (TEM), Fourier transform infrared (FT-IR) spectroscopy and ultraviolet–visible (UV–vis) spectroscopy were used to demonstrate the successful attachment of Fe_3O_4 nanoparticles to graphene and graphene oxide sheets. It is shown that the Fe_3O_4 nanoparticles with a size of *ca.* 60 nm were well spread out on the graphene and graphene oxide sheets, respectively. The thermal stability of the nanocomposites was investigated by thermogravimetry (TG) and differential scanning calorimetry (DSC) analyses. Magnetic studies reveal a superparamagnetic behavior of the graphene/Fe_3O_4 nanocomposites, which make it promising for practical applications in future bio-nanotechnology.

1. Introduction

Since discovered in 2004, graphene—a single 2D carbon sheet with the same structure as the individual layers in graphite, has been attracting more and more attention from scientific community and nowadays has become a sparkling rising star on the horizon of nanomaterials science, due to its extraordinary electrical, thermal, and mechanical properties [1–3]. Graphene-based nanocomposites, for their superb properties, have emerged as quite intriguing materials that hold promise for many applications. When incorporated graphene into polymer [4–7] or ceramic [8,9] matrices, its peculiar properties manifest as remarkable improvements in the host material. On the other hand, the dispersion of inorganic nanoparticles on graphene sheets provides a new way to further explore the potential application of graphene-based materials. So far, numerous graphene/inorganic nanocomposites, derived from the decoration of graphene sheets with inorganic nanoparticles (NPs) such as metal, metal oxide and sulfide, have been successfully synthesized [10–19].

In recent years, magnetic nanoparticles are of great interest for researchers from a wide range of disciplines, including magnetic fluids [20], data storage [21], biotechnology/biomedicine [22], catalysis [23,24], magnetic resonance imaging [25,26], environmental remediation [27,28], etc. Among them, magnetite Fe_3O_4 nanoparticles possess the most interesting properties because of the presence of iron cations in two valence states, Fe^{2+} and Fe^{3+}, in the inverse spinel structure. It is well known that fruitful research has been made into the preparation of carbon nanotube (CNT)/Fe_3O_4 nanocomposites, which are of many potential applications ranging from electromagnetic devices to magnetically guided drug delivery systems [29,30]. In comparison with CNTs, graphene possesses similar physical properties but larger surface areas, which can be considered as an unrolled CNT [31,32]. In addition, the production cost of graphene sheets in large quantities is much lower than that of CNTs [4,33]. Therefore, graphene as a low cost alternative to CNTs in nanocomposites is highly expected [34].

In recent researches, Chen and co-workers [35] synthesized a superparamagnetic graphene oxide/Fe_3O_4 nanocomposites via a chemical precipitation method, which demonstrated potential application in controlled targeted drug delivery and release. Ye and co-workers [36] synthesized graphene oxide/Fe_3O_4 nanocomposites through a high temperature reaction of ferric triacetylacetonate with graphene oxide in 1-methyl-2-pyrrolidone solution. Yu and co-workers [37] successfully deposited Fe_3O_4 nanoparticles onto poly(sodium 4-styrenesulfonate)(PSS)-coated graphene through a high temperature reflux process at 278 °C under argon protection. In this paper, we present one facile one-pot solvothermal approach for the large-scale syntheses of graphene/Fe_3O_4 and graphene oxide/Fe_3O_4 nanocomposites. The thermal and magnetic properties of the products were investigated.

* Corresponding author. Tel.: +86 511 84401889; fax: +86 511 88791800.
E-mail address: xiaopingshen@163.com (X. Shen).

0925-8388/$ – see front matter © 2010 Elsevier B.V. All rights reserved.
doi:10.1016/j.jallcom.2010.06.158

2. Experimental

2.1. Materials and measurements

All chemicals used in our experiments were reagent grade and used without further purification. The precursor of iron acetylacetonate [$Fe(acac)_3$] was synthesized according to the literature method [38]. The morphology and structure of the products were determined by transmission electron microscopy (TEM, JEM—2100) and X-ray diffraction (XRD, D/MAX2500, Rigaka) with Cu Kα radiation. Samples for TEM were prepared by dropping the products on a carbon-coated copper grid after ultrasonic dispersing in absolute ethanol. Fourier transform infrared (FT-IR) spectra were recorded on a Nicolet FT-170SX spectrometer with KBr pellets in the 4000–400 cm^{-1} region. Ultraviolet–visible (UV–vis) spectroscopy measurements were performed on a UV-2450 ultraviolet–visible spectrophotometer in water dispersions. The differential scanning calorimetry (DSC) and thermogravimetry (TG) measurements were carried out with a NETZSCH STA449C thermal analyzer, which allows simultaneous TG and DSC measurements. The magnetic measurements were performed using a Quantum Design MPMS-XL SQUID magnetometer.

2.2. Synthesis of graphite oxide (GO)

The preparation of graphite oxide (GO) was carried out by a modified Hummers method [39]. In a typical synthesis, 2.0 g of graphite powder was put into cold (0 °C) concentrated H_2SO_4 (100 mL). Then, $KMnO_4$ (8.0 g) was added gradually under stirring and the temperature of the mixture was kept to be below 10 °C by cooling. The reaction mixture was continued for 2 h at the temperature below 10 °C. Successively, the mixture was stirred at 35 °C for 1 h, and then diluted with 100 mL of deionized (DI) water. Because the addition of water in concentrated sulfuric acid medium released a large amount of heat, the addition of water was performed in an ice bath to keep the temperature below 100 °C. After adding all of the 100 mL of DI water, the mixture was stirred for 1 h, and was then further diluted to approximately 300 mL with DI water. After that, 20 mL of 30% H_2O_2 was added to the mixture to reduce the residual $KMnO_4$. The mixture released a large amount of bubbles and the color of the mixture changed into brilliant yellow. Finally, the mixture was filtered and washed with 5% HCl aqueous solution (800 mL) to remove metal ions followed by 1.0 L of DI water to remove the acid. The resulting solid was dried at 60 °C for 24 h. For further purification, the as-obtained graphite oxide was re-dispersed in DI water and then was dialyzed for 1 week to remove residual salts and acids.

2.3. Syntheses of graphene-based magnetic nanocomposites

Graphene/Fe_3O_4 nanocomposites: 20 mg of graphite oxide and 200 mg of iron acetylacetonate ($Fe(acac)_3$) were dispersed in 45 mL of ethylene glycol (EG) with ultrasonication for 30 min, 20 μL of hydrazine hydrate was slowly added into the mixture with stirring. Subsequently, the mixture was put into an autoclave and heated at 180 °C for 16 h. The as-synthesized product was isolated by centrifugation, washed three times with water and ethanol, respectively, and finally dried in a vacuum oven at 60 °C. For graphene oxide/Fe_3O_4 nanocomposites, the synthesis was carried out in the absence of hydrazine hydrate under the same other conditions as the graphene/Fe_3O_4.

3. Results and discussion

X-ray diffraction (XRD) measurements were employed to investigate the phase and structure of the synthesized samples. As shown in Fig. 1, the XRD pattern of the as-prepared graphite oxide (Fig. 1a) shows a sharp peak at $2\theta = 10.2°$, corresponding to the (0 0 1) reflection of graphite oxide [40]. From Fig. 1b, except the diffraction peak at $2\theta = 10.9°$ resulted from graphite oxide, all the diffraction peaks of the graphene oxide/Fe_3O_4 sample can be indexed to cubic Fe_3O_4 (JCPDS: 65-3107), which are broadened owing to the small sizes of the Fe_3O_4 particles. The XRD pattern of the graphene/Fe_3O_4 sample is shown in Fig. 1c, it can be seen that except the peaks assigned to Fe_3O_4, no any diffraction peaks resulted from graphite oxide and/or graphite can be found, suggesting that the graphene oxide was effectively reduced into graphene and the self-restacking of the as-reduced graphene sheets was well prevented.

Fig. 2 shows the FT-IR spectra of the GO and as-synthesized nanocomposites. The oxygen-containing functional groups of GO were revealed by the bands at 1057, 1230, 1400 and 1732 cm^{-1} (Fig. 2a), which correspond to C–O stretching vibrations, C–OH stretching peak, C–O–H deformation peak and C=O stretching of COOH groups, respectively. The peak at 1618 cm^{-1} can be assigned to the skeletal vibrations of unoxidized graphitic domains [33]. All

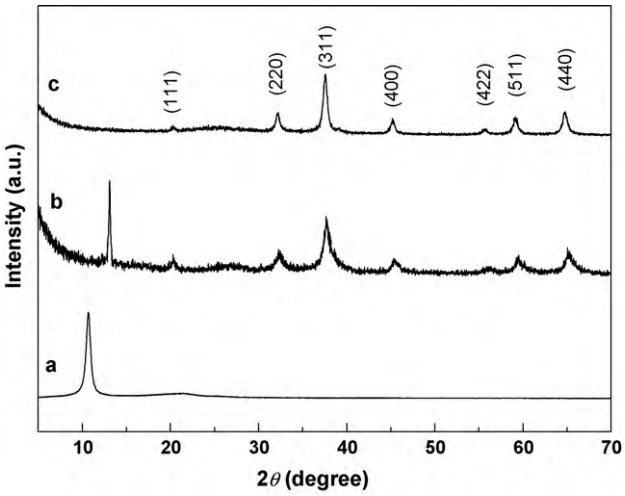

Fig. 1. XRD patterns of (a) graphite oxide, (b) graphene oxide/Fe_3O_4 and (c) graphene/Fe_3O_4 nanocomposites.

these bands related with the oxygen-containing functional groups almost remain in the FT-IR spectrum of the graphene oxide/Fe_3O_4 (Fig. 2b), while almost vanish in the graphene/Fe_3O_4 (Fig. 2c), revealing that these oxygen-containing functional groups were removed in the presence of hydrazine hydrate, and accordingly the graphene oxide was reduced into graphene by hydrazine hydrate. Moreover, an additional peak at *ca.* 600 cm^{-1} in Fig. 2b and c can be ascribed to lattice absorption of Fe_3O_4, further confirming the existence of Fe_3O_4 [37]. Therefore, although hydrazine hydrate was necessary to transform graphene oxide into graphene, it had hardly any effect on the formation of Fe_3O_4 in the present syntheses.

Transmission electron microscopy (TEM) and high resolution transmission electron microscopy (HRTEM) analyses were performed on the as-prepared product to determine their features in nanometer domain. Fig. 3 shows the TEM images of the graphene oxide/Fe_3O_4 composites. It can be seen that the Fe_3O_4 nanoparticles with a size of about 60 nm were well distributed on graphene oxide sheets, which were nearly flat and had a big area up to several square micrometers. Some nanoparticles were slightly aggregated due to the loading degree close to saturation. The TEM images of graphene/Fe_3O_4 were shown in Fig. 4. It can be clearly seen that the

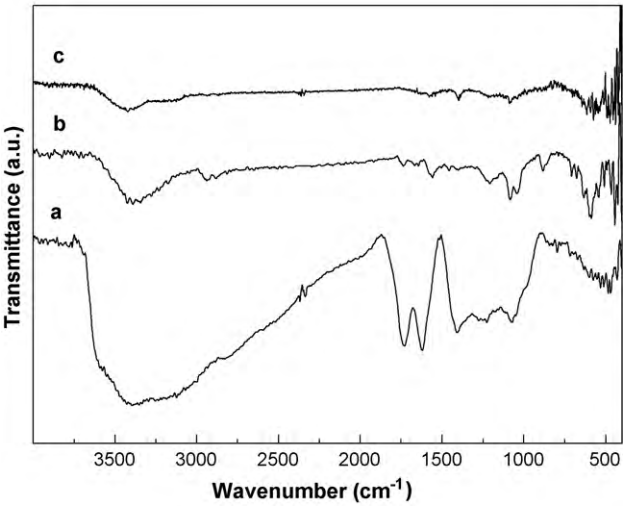

Fig. 2. FT-IR spectra of (a) graphite oxide, (b) graphene oxide/Fe_3O_4 and (c) graphene/Fe_3O_4 nanocomposites.

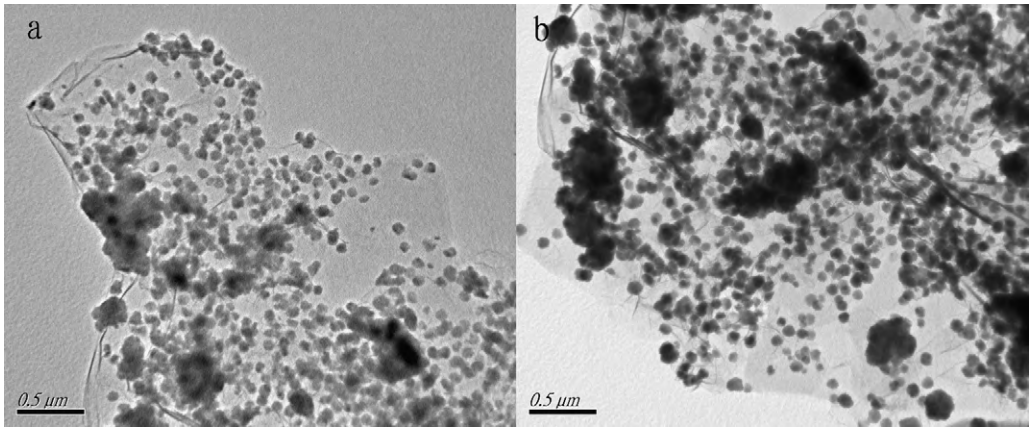

Fig. 3. TEM images of the graphene oxide/Fe_3O_4 nanocomposite.

crumpled silk waves-like carbon sheets, a characteristic feature of the single-layer graphene sheets, were well decorated by uniform Fe_3O_4 nanoparticles (Fig. 4a), and almost no Fe_3O_4 nanoparticles were found outside of the graphene sheets. As shown in Fig. 4b, the Fe_3O_4 nanoparticles have a size of about 60 nm and consist of a large number of tiny Fe_3O_4 nanocrystals with a size of only 2–3 nm. The HRTEM image shown in Fig. 4c also reveals the polycrystalline structure of the Fe_3O_4 nanoparticles, and the lattice fringes with interplanar distances of 0.25 nm and 0.21 nm can be assigned to the (3 1 1) and (4 0 0) planes of the cubic Fe_3O_4, respectively. The selected-area electron diffraction pattern (SAED) (Fig. 4d) clearly shows the ring pattern arising from the cubic Fe_3O_4 [41], further confirming the polycrystalline nature of Fe_3O_4 nanoparticles.

Fig. 5 shows the UV–vis absorption spectra of the as-synthesized nanocomposites, together with pure graphene for comparison. For the UV–vis measurements, the samples were dispersed in water by sonication. It can be seen that the graphene (Fig. 5a) shows a strong absorption peak at 265 nm, together with a weak shoulder peak at *ca.* 223 nm. The absorption peak at 265 nm is generally regarded as the excitation of π-plasmon of graphitic structure [42]. We also see the corresponding broadening absorption peak at 265 nm in both the graphene oxide/Fe_3O_4 and the graphene/Fe_3O_4 (Fig. 5b and c). Interestingly, both the graphene oxide/Fe_3O_4 and the graphene/Fe_3O_4 show a strong new absorption peak at 214 nm, probably arising from the coupling between graphene sheet and Fe_3O_4 nanoparticles.

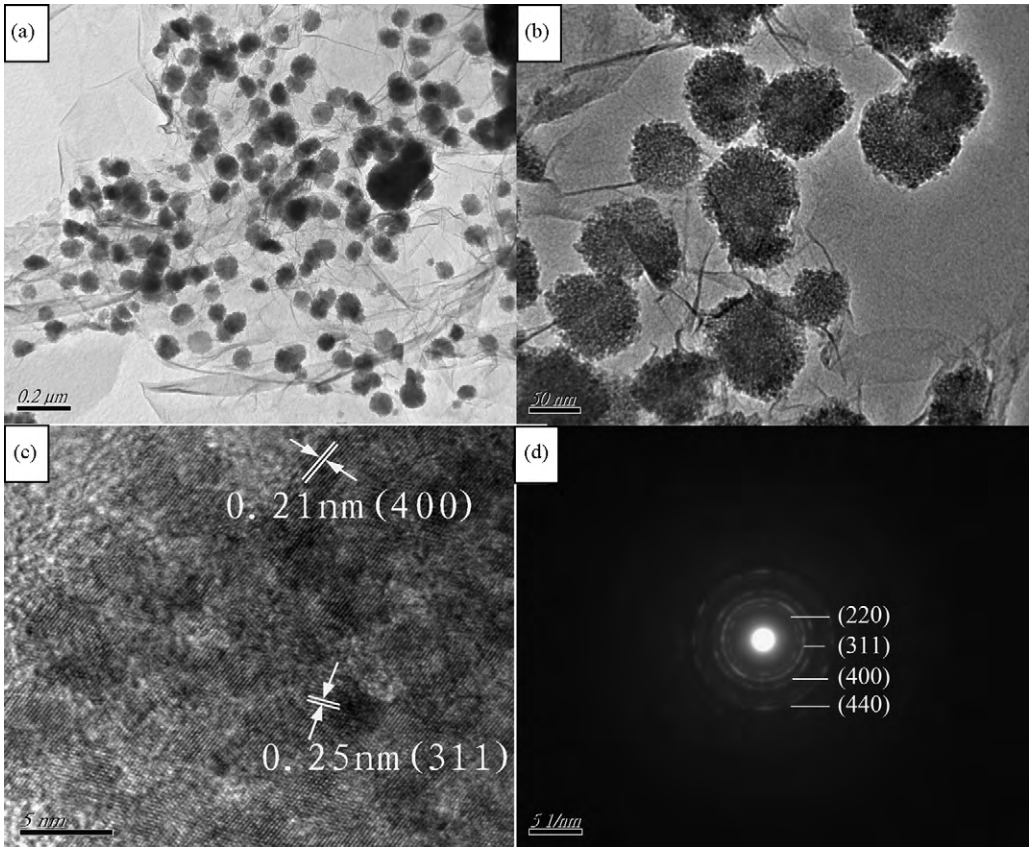

Fig. 4. (a and b) TEM, (c) HRTEM and (d) SAED images of the graphene/Fe_3O_4 nanocomposites.

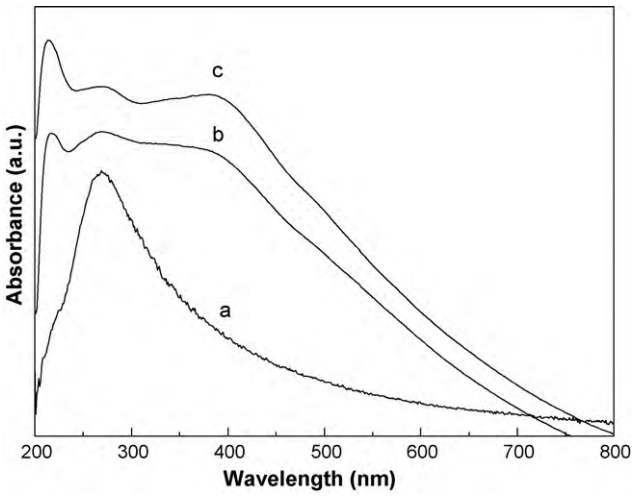

Fig. 5. UV–vis spectra of (a) the graphene sheets, (b) graphene oxide/Fe_3O_4 and (c) graphene/Fe_3O_4 nanocomposites.

The TG–DSC measurement was performed under nitrogen atmosphere with a heating rate of 10 °C min^{-1}. As shown in Fig. 6a, with increasing temperature, the graphene oxide/Fe_3O_4 shows a gradual weight loss up to 410 °C. Then, an abrupt weight loss happens at 410–450 °C and the weight loss at 450 °C is about 37%. Correspondingly, the DSC curve shows a strong exothermal peak centered at *ca.* 420 °C, which can be attributed to the decomposition and vaporization of various labile oxygen functional groups of GO. From Fig. 6b, it can be seen that with increasing temperature, the graphene/Fe_3O_4 shows a gradual weight loss up to 900 °C, and no abrupt weight loss and obvious exothermal peak can be observed. This is consistent with the thermal behavior of graphene in N_2 atmosphere as reported in the literatures [43,44], confirming that the thermal stability of the graphene derived from chemical reduction of GO is much lower than that of the bulk graphite powders [45]. The weight loss is usually attributed to the loss of the residual (or absorbed) solvent and the decomposition of residual organic functional groups on graphenes [10,44].

The magnetic measurements were performed on the graphene/Fe_3O_4 nanocomposites using a Quantum Design MPMS-XL SQUID magnetometer. The field dependence of the magnetization measured at 300 K is shown in Fig. 7a. It can be seen that the magnetization first increases sharply and then gradually with the increase of the applied field, and reaches saturation

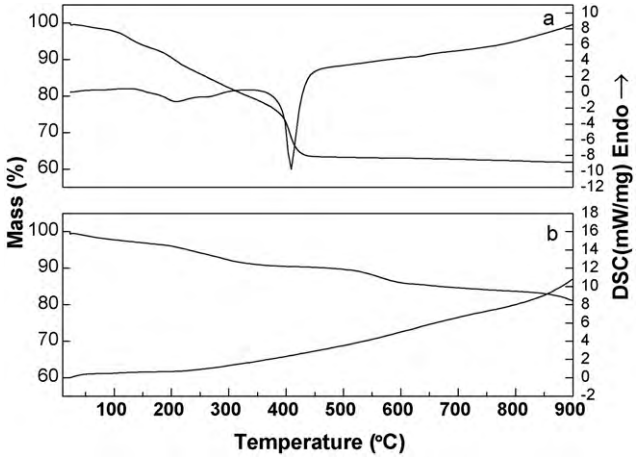

Fig. 6. TG–DSC curves of (a) graphene oxide/Fe_3O_4 and (b) graphene/Fe_3O_4 nanocomposites.

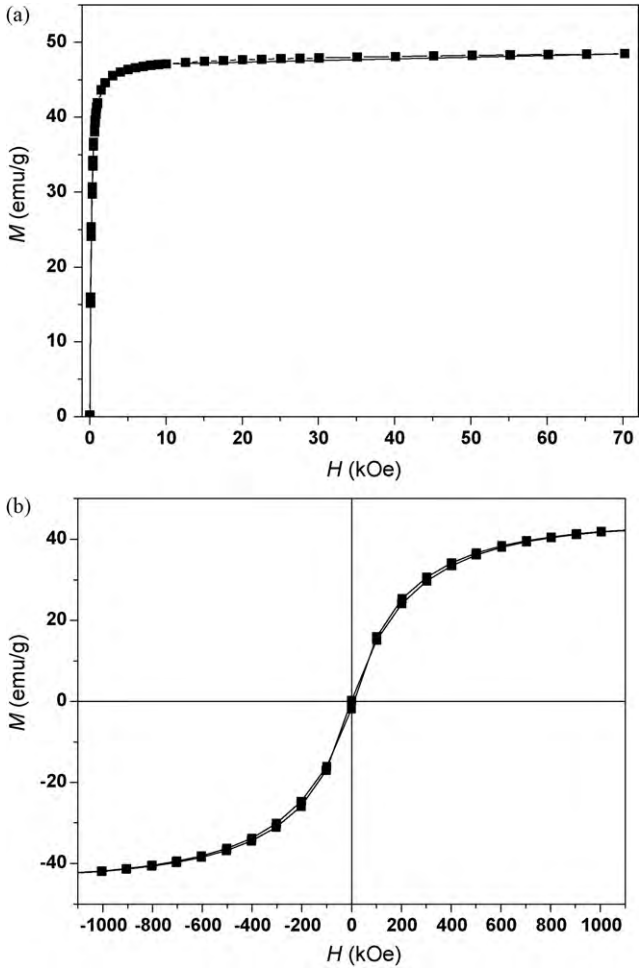

Fig. 7. (a) Field dependence of the magnetization and (b) magnetic hysteresis loop for the graphene/Fe_3O_4 nanocomposites at 300 K.

in *ca.* 5 kOe. The saturation magnetization of the composite is 48.5 emu/g, which is smaller than the reported value of bulk Fe_3O_4 of 92 emu/g. This can be attributed to the small particles size and relatively low amount of the Fe_3O_4 in the composite [46–48]. As shown in Fig. 7b, the graphene/Fe_3O_4 nanocomposites show no obvious magnetic hysteresis loop at 300 K, indicating a superparamagnetic behavior, which is consistent with the ultrafine nature of the Fe_3O_4 nanocrystals loaded on graphene sheets [47,48].

4. Conclusions

In conclusion, graphene-based magnetic nanocomposites of graphene/Fe_3O_4 and graphene oxide/Fe_3O_4 have been successfully synthesized by a facile one-pot solvothermal method in EG medium. The Fe_3O_4 nanoparticles with a size of about 60 nm were well attached on graphene sheets and effectively prevented the graphene sheets from stacking together. The graphene/Fe_3O_4 nanocomposites with superparamagnetic property provide an opportunity for the applications in the fields of biomedicine, biomaterials separation and biodiagnostics. Detailed studies on these applications are underway.

Acknowledgements

The authors are grateful for financial support from the Natural Science Foundation of Jiangsu Province (No. BK2009196) and the Advanced Talent Foundation of Jiangsu University (No. 05JDG043).

References

[1] K.S. Novoselov, A.K. Geim, S.V. Morozov, D. Jiang, Y. Zhang, S.V. Dubonos, I.V. Grigorieva, A.A. Firsov, Science 306 (2004) 666–669.
[2] R. Van Noorden, Nature 442 (2006) 228–229.
[3] A.K. Geim, K.S. Novoselov, Nat. Mater. 6 (2007) 183–191.
[4] S. Stankovich, D.A. Dikin, G.H.B. Dommett, K.M. Kohlhaas, E.J. Zimney, E.A. Stach, R.D. Piner, S.T. Nguyen, R.S. Ruoff, Nature 442 (2006) 282–286.
[5] T. Ramanathan, A.A. Abdala, S. Stankovich, D.A. Dikin, M. Herrera-Alonso, R.D. Piner, D.H. Adamson, H.C. Schniepp, X. Chen, R.S. Ruoff, S.T. Nguyen, I.A. Aksay, R.K. Prud'homme, L.C. Brinson, Nat. Nanotechnol. 3 (2008) 327–331.
[6] J.J. Liang, Y. Wang, Y. Huang, Y.F. Ma, Z.F. Liu, F.M. Cai, C.D. Zhang, H.J. Gao, Y.S. Chen, Carbon 47 (2008) 922–925.
[7] N. Liu, F. Luo, H.X. Wu, Y.H. Liu, C. Zhang, J. Chen, Adv. Funct. Mater. 18 (2008) 1518–1525.
[8] S. Watcharotone, D.A. Dikin, S. Stankovich, R. Piner, I. Jung, G.H.B. Dommett, G. Evmenenko, S.E. Wu, S. Chen, C.P. Liu, S.T. Nguyen, R.S. Ruoff, Nano Lett. 7 (2007) 1888–1892.
[9] Y.C. Fan, L.J. Wang, J.L. Li, J.Q. Li, S.K. Sun, F. Chen, L.D. Chen, W. Jiang, Carbon 48 (2010) 1743–1749.
[10] C. Xu, X. Wang, J.W. Zhu, J. Phys. Chem. C 112 (2008) 19841–19845.
[11] M. Ryan, B. Seger, P.V. Kamat, J. Phys. Chem. C 112 (2008) 5263–5266.
[12] G.X. Wang, B. Wang, X.L. Wang, J. Park, S.X. Dou, H.J. Ahn, K. Kim, J. Mater. Chem. 19 (2009) 8378–8384.
[13] G. Williams, B. Seger, P.V. Kamat, ACS Nano 2 (2008) 1487–1491.
[14] I.V. Lightcap, T.H. Kosel, P.V. Kamat, Nano Lett. 10 (2010) 577–583.
[15] J. Yao, X.P. Shen, B. Wang, H.K. Liu, G.X. Wang, Electrochem. Commun. 11 (2009) 1849–1852.
[16] Y.C. Si, E.T. Samulski, Chem. Mater. 20 (2008) 6792–6797.
[17] S.M. Paek, E.J. Yoo, I. Honma, Nano Lett. 9 (2009) 72–75.
[18] C. Nethravathi, T. Nisha, N. Ravishankar, C. Shivakumara, M. Rajamathi, Carbon 47 (2009) 2054–2059.
[19] D.H. Wang, D.W. Choi, J. Li, Z.G. Yang, Z.M. Nie, R. Kou, D.H. Hu, C.M. Wang, L.V. Saraf, J.G. Zhang, I.A. Aksay, J. Liu, ACS Nano 3 (2009) 907–914.
[20] S. Chikazumi, S. Taketomi, M. Ukita, M. Mizukami, H. Miyajima, M. Setogawa, Y. Kurihara, J. Magn. Magn. Mater. 65 (1987) 245–251.
[21] D. Chiba, M. Sawicki, Y. Nishitani, Y. Nakatani, F. Matsukura, H. Ohno, Nature 455 (2008) 515–518.
[22] A.K. Gupta, M. Gupta, Biomaterials 26 (2005) 3995–4021.
[23] A.H. Lu, W. Schmidt, N. Matoussevitch, H. Bpnnermann, B. Spliethoff, B. Tesche, E. Bill, W. Kiefer, F. Schuth, Angew. Chem. Int. Ed. 43 (2004) 4303–4306.
[24] S.C. Tsang, V. Caps, I. Paraskevas, D. Chadwick, D. Thompsett, Angew. Chem. Int. Ed. 43 (2004) 5645–5649.
[25] S. Mornet, S. Vasseur, F. Grasset, P. Verveka, P. Goglio, A. Demourgues, J. Portier, E. Pollert, E. Duguet, Prog. Solid State Chem. 34 (2006) 237–247.
[26] Z. Li, L. Wei, M.Y. Gao, H. Lei, Adv. Mater. 17 (2005) 1001–1006.
[27] D.W. Elliott, W.X. Zhang, Environ. Sci. Technol. 35 (2001) 4922–4926.
[28] M. Takafuji, S. Ide, H. Ihara, Z. Xu, Chem. Mater. 16 (2004) 1977–1983.
[29] S. Qu, J. Wang, J.L. Kong, P.Y. Yang, G. Chen, Talanta 71 (2007) 1096–1102.
[30] Z. Huang, J. Li, Q.W. Chen, H. Wang, Mater. Chem. Phys. 114 (2009) 33–36.
[31] S. Niyogi, E. Bekyarova, M.E. Itkis, J.L. McWilliams, M.A. Hamon, R.C. Haddon, J. Am. Chem. Soc. 128 (2006) 7720–7721.
[32] D.A. Dikin, S. Stankovich, E.J. Zimney, R.D. Piner, G.H.B. Dommett, G. Evmenenko, S.T. Nguyen, R.S. Ruoff, Nature 448 (2007) 457–460.
[33] Y.X. Xu, H. Bai, G.W. Lu, C. Li, G.Q. Shi, J. Am. Chem. Soc. 130 (2008) 5856–5857.
[34] X. Lv, Y. Huang, Z.B. Liu, J.G. Tian, Y. Wang, Y.F. Ma, J.J. Liang, S.P. Fu, X.J. Wan, Y.S. Chen, Small 5 (2009) 1682–1687.
[35] X.Y. Yang, X.Y. Zhang, Y.F. Ma, Y. Huang, Y.S. Wang, Y.S. Chen, J. Mater. Chem. 19 (2009) 2710–2714.
[36] J.F. Shen, Y.Z. Hu, M. Shi, N. Li, H.W. Ma, M.X. Ye, J. Phys. Chem. C 114 (2010) 1498–1503.
[37] H.P. Cong, J.J. He, Y. Lu, S.H. Yu, Small 6 (2010) 169–173.
[38] R.G. Charles, M.A. Pawlikowski, J. Phys. Chem. 62 (1958) 440–444.
[39] J.L. Wu, X.P. Shen, L. Jiang, K. Wang, K.M. Chen, Appl. Surf. Sci. 256 (2010) 2826–2830.
[40] T. Nakajima, A. Mabuchi, R. Hagiwara, Carbon 26 (1988) 357–361.
[41] H.Q. Cao, M.F. Zhu, Y.G. Li, J. Solid State Chem. 179 (2006) 1208–1213.
[42] X. Wang, L.J. Zhi, N. Tsao, J.L. Tomovic, K. Mullen, Angew. Chem. Int. Ed. 47 (2008) 2990–2992.
[43] X.B. Fan, W.C. Peng, Y. Li, X.Y. Li, S.L. Wang, G.L. Zhang, F.B. Zhang, Adv. Mater. 20 (2008) 4490–4493.
[44] S. Stankovich, D. Dikin, R.D. Piner, K.A. Kohlhaas, A. Kleinhammes, Y. Jia, Y. Wu, S.T. Nguyen, R.S. Ruoff, Carbon 45 (2007) 1558–1565.
[45] G.X. Wang, J. Yang, J. Park, X.L. Gou, B. Wang, H. Liu, J. Yao, J. Phys. Chem. C 112 (2008) 8192–8195.
[46] D.H. Han, J.P. Wang, H.L. Luo, J. Magn. Magn. Mater. 136 (1994) 176–182.
[47] J.Q. Wang, W. Cai, J.T. Feng, X.X. Meng, E.Z. Liu, J. Mater. Chem. 17 (2007) 1188–1192.
[48] R.N. Panda, N.S. Gajbhiye, G. Balaji, J. Alloys Compd. 326 (2001) 50–53.